Penetrant competition and plasticization in membranes: How negatives can be positives in natural gas sweetening

Penetrant competition and plasticization in membranes: how negatives can be positives in natural gas sweetening

Yang Liu[a], *Zhijie Chen*[b], *Wulin Qiu*[a], *Gongping Liu*[a], *Mohamed Eddaoudi*[b,*], *William J. Koros*[a,*]

[a]School of Chemical and Biomolecular Engineering, Georgia Institute of Technology, 311 Ferst Dr. NW, Atlanta, GA, 30032, USA

[b]Advanced Membranes and Porous Materials Center, Division of Physical Science and Engineering, King Abdullah University of Science and Technology, Thuwal 23955-6900, KSA

[*]Corresponding authors: wjk@chbe.gatech.edu (W.J.K.); mohamed.eddaoudi@kaust.edu.sa (M.E.)

ABSTRACT

Membranes are attractive for upgrading natural gas; however, the gas permeation processes through membranes are challenging to control. The coexistence of condensable H_2S and CO_2 typically causes membrane performance to decline under practical feed conditions, due to uncontrolled penetrate competition and undesired plasticization of the membrane polymer matrix. In this paper, we report a strategy to successfully transform these apparent negatives, i.e. plasticization and penetrate competition, into positives that boost the natural gas sweetening efficiency of membranes greatly. Our strategy is to disperse engineered metal organic framework (MOF) fillers into designed polymer matrices to form hybrid membranes, which promote the permeation of both H_2S and CO_2 but hinder CH_4 permeation. Moreover, uniformly dispersed MOF fillers also significantly alter the plasticization responses of polymer matrices, enabling controlled plasticization benefits. Ultimately, we illustrate a highly tunable MOF-polymer hybrid

membrane platform that meets the diverse natural gas sweetening requirements under aggressive conditions.

Keywords: hydrogen sulfide; carbon dioxide; mixed matrix membranes; metal-organic frameworks

Introduction

Methane (CH_4) typically comprises from 50% - 90% of natural gas; however, a significant amount of undesirable impurities, e.g. hydrogen sulfide (H_2S) and carbon dioxide (CO_2), are also present in many natural gas reservoirs [1-3]. Natural gas with more than 4 part per million (ppm) H_2S by volume is considered "sour", and H_2S concentrations in many worldwide natural gas reservoirs range from hundreds of ppm to 30 mol.% (Middle East) [4]. Raw natural gas must be "sweetened" to remove H_2S and CO_2 from the product (CH_4) to meet pipeline specifications, e.g. < 4 ppm (H_2S) and < 2 % (CO_2) in the U.S., for transportation and use [1]. Current thermally-driven amine absorption methods for sweetening are highly energy-intensive and have high capital and operating costs [1,5]. Membrane separations can potentially offer higher energy efficiency than such thermally-driven methods as well as compact footprints [6-9] and easy scale-up [10,11]. Currently, however, membranes cannot meet *simultaneous* (H_2S+CO_2) removal targets, i.e. $\alpha_{H2S/CH4} > 30$ and $\alpha_{CO2/CH4} > 20$ (where α represents permselectivity) [1], along with attractive H_2S and CO_2 intrinsic permeabilities, typically > 100 barrer for each of the acidic component [3,12,13]. A new generation of membranes allowing simultaneous efficient removal

of H_2S and CO_2 from natural gas reservoirs in realistic conditions, typically > 50 bar, are therefore needed and are considered in this paper to meet these simultaneous needs.

Achieving simultaneous (H_2S+CO_2) removal targets for natural gas requires tuning and balancing sorption and diffusion advantages for the rather different H_2S/CH_4 and CO_2/CH_4 gas pairs. Fortunately, as described herein, the H_2S and CO_2 can even cooperate to "beat" CH_4 in the permeation process based on differences in *condensability* (H_2S > CO_2 > CH_4) and *molecular size* (CO_2 < H_2S < CH_4). This attractive outcome is possible by using the combination of characteristics of the H_2S/CH_4 and CO_2/CH_4 pairs by careful design of both intrinsic membrane propererties and tunable operating conditions. These facts are the basis for our strategy to achieve exceptional H_2S/CH_4 and CO_2/CH_4 selectivities simultaneously. Penetrant competitions [14] for sorption sites and diffusion paths within an engineered membrane can offer sorption advantages for H_2S vs. CH_4 without undermining the diffusion advantage of CO_2 vs. CH_4, and vice versa. However, in practice, membranes favoring H_2S-removal usually show less attractive CO_2-removal efficiency and vice verse [15] (Figure S1) due to the fact that penetrant competitions are poorly controlled in currently available membrane materials.

Glassy polymer membranes are ideal platforms to apply the above approach if controlled swelling can be used to engineer sorption dominated H_2S/CH_4 factors and diffusion dominated CO_2/CH_4 factors for high-pressure feeds [16]. Polymer functionalization using specific groups favoring H_2S and CO_2 sorption can, in principle, further promote their sorption advantages over CH_4; moreover, their intrinsic molecular discrimination feature still advances the CO_2/CH_4 separation. Nevertheless, achieving this goal requires *avoiding excessive matrix plasticization* that undermines control of the (sorption + diffusion) advantages of (H_2S+CO_2) over CH_4 [17].

Crosslinking of glassy polymers avoids excessive plasticization [12,17], and controlling attractions of added functional groups with targeted desired penetrants can be done in principle [18], but this strategy is difficult to implement in highly selective (H_2S+CO_2)/CH_4 separations.

Fortunately, another tool can be used, wherein incorporating metal-organic frameworks (MOFs) into glassy polymer membranes [19] for (H_2S+CO_2) separation allows engineering penetrant competition and plasticization (Figure 1). MOFs are microporous crystalline materials with highly tunable functionalities and pore-aperture sizes [20-23], which can promote both H_2S/CH_4 and CO_2/CH_4 separations by tuning the molecular competitions among H_2S, CO_2 and CH_4 (Figure 1b). Scale-up of pure MOF membranes to large economical modules remains a challenge [24]; however, the formation of polymer-MOF hybrid "mixed matrix" membranes has been demonstrated [25]. Moreover, excessive plasticization of glassy polymers is inhibited by the incorporated "rigid" MOF fillers [26] even without crosslinking while allowing some desirable swelling of the polymer chains to benefit productivity (Figure 1c). Combining these advantages, herein, we obtained extremely high selectivities for both H_2S/CH_4 (>> 30) and CO_2/CH_4 (>> 20) separations along with excellent H_2S and CO_2 permeabilities (>> 100 barrer). Furthermore, the H_2S and CO_2 removal efficiencies are *highly tailorable*, meeting the critical separation requirements under various realistic natural gas sweetening conditions.

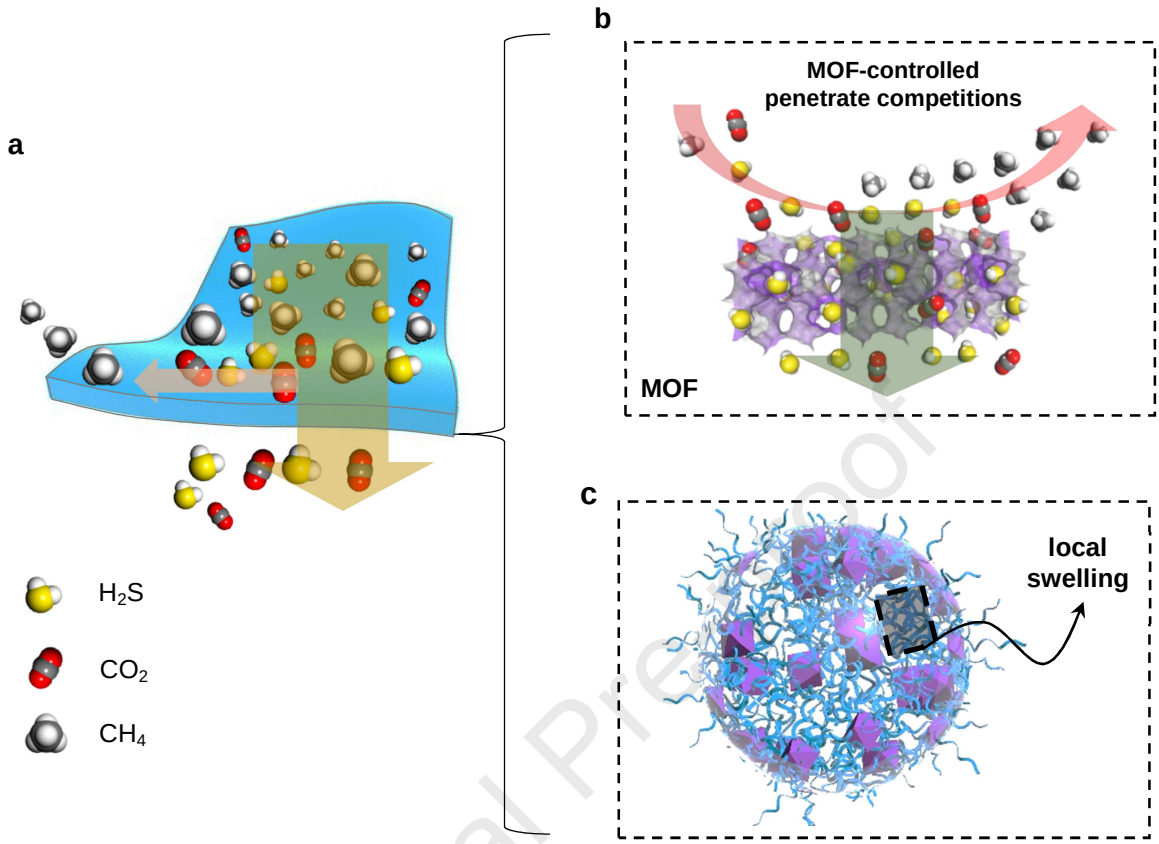

Figure 1. MOF-polymer hybrid membranes for natural gas sweetening. (a) Illustration of the concept of membrane-based natural gas sweetening. (b) MOF-controlled penetrate competitions for enhancing the competitive permeation strength of H_2S and CO_2 over CH_4. (c) Dispersed MOF fillers (purple octahedron) prevent excessive swelling of the polymer matrix (cyan chains), while desirable plasticization benefits [16] can still be achieved by the controlled local swelling of the polymer matrix.

Methods

Synthesis of M-fcu-MOF. The synthesis of MOF materials are same or slightly modified according to literatures. *(1)* *Zr-fum-**fcu**-MOF* [27]: fumaric acid (81 mg, 0.7 mmol), $ZrOCl_2 \cdot 8H_2O$ (230 mg, 0.7 mmol), formic acid (2.65 mL, 70 mmol), and DMF (18 mL) were dissolved in a sealed vial followed by placing into a preheated (120 °C) oven for 24 h. The vial

was cooled to room temperature, and the products were collected by centrifugation. The sample was washed 6 times over 3 days with 45 mL of anhydrous DMF and then sequentially immersed in 45 mL of methanol for 3 days, during which time the methanol was replaced 2 times per day. *(2) Y-fum-**fcu**-MOF* [28]: *fum*aric acid (10.1 mg, 0.087 mmol), $Y(NO_3)_3 \cdot 6H_2O$ (33.4 mg, 0.087 mmol), 2-fluorobenzoic acid (195.0 mg, 1.392 mmol) dimethylformamide (DMF) (2.7 mL), and deionized H_2O (0.7 mL), were combined in a 20 ml scintillation vial, sealed and heated to 115°C for 72 h. The collected solid was dried at 150°C under vacuum for 24 h to yield activated samples. *(3) Zr-mfum-**fcu**-MOF* [29]: mesaconic acid (91 mg, 0.7 mmol),), $ZrOCl_2 \cdot 8H_2O$ (230 mg, 0.7 mmol), formic acid (2.65 mL, 70 mmol), and DMF (18 mL) were dissolved in a sealed vial followed by placing into a preheated (120 °C) oven for 24 h. The vial was cooled to room temperature, and the products were collected by centrifugation. The sample was washed 6 times over 3 days with 45 mL of anhydrous DMF and then sequentially immersed in 45 mL of methanol for 3 days, during which time the methanol was replaced 2 times per day.

Synthesis of polymers. Both 6FDA/BPDA-DAM_1:1 and 6FDA/ODPA-DAM_1:1 were synthesized via condensation of the dianhydrides with diamine in a mole ratio of 1:1, followed by chemical imidization. The (4,4'-hexafluoroisopropylidene) diphthalic anhydride (6FDA), 3,3',4,4'-biphenyl dianhydride (BPDA), 4,4'-oxydiphthalic dianhydride (ODPA), and diaminomesitylene (DAM) were purchased from Aldrich. First of all, the dianhydrides and DAM were dried under vacuum at 120 ^oC and 55 ^oC, respectively. Meanwhile, the solvents, including 1-methyl-2-pyrrolidinone (NMP), acetic anhydride (AcAn), and beta picoline, were dried with pre-dried molecular sieves, while the reactor was pre-dried with continuous N_2 purging. Secondly, a designated amount of DAM was dissolved in half amount of the total NMP under stirring until DAM dissolved completely. The dianhydrides mixture (6FDA/BPDA or

6FDA/ODPA) was then gradually added into the reactor, forming a polymer solution with a concentration of ~20 wt%. The temperature of the solution was maintained below 5 ^{o}C using a cooling bath. Thirdly, the chemical imidization was carried out at room temperature. The beta-picoline (10 grams/0.1 mol dianhydride) and AcAn (10 times of picoline in grams) were added to the solution under stirring with N_2 purging for 24 hr. The solution was quenched into methanol, chopped into powder, filtered, washed thoroughly with methanol. Finally, the resulting polyimide powder were evaporated at room temperature overnight to remove the solvent and were further dried under vacuum at 220 ^{o}C for 24 hr. 6FDA-DAM and 6FDA-DAM/DABA_3:2 polyimides were purchased from Akron Polymer Systems, Inc.

Membrane Preparation. *(1) 6FDA-polyimide membranes.* 6FDA-polyimides were dried in a vacuum oven at 110 °C for 12 hr before being dissolved in THF to form 15 wt% polyimide/THF mixtures. The solutions were mixed on a rolling mixer for 24 hr to dissolve the polymer. The resulting casting solutions were poured onto a glass plate in a THF pre-saturated glove bag. Pure 6FDA-polyimide dense films were formed by casting the dope using a draw knife. The films were left in the glove bag for 18 h to allow the THF solvent to evaporate slowly and then dried in a vacuum oven at 200 °C for 24 h. *(2) M-**fcu**-MOF/6FDA-polyimide hybrid membranes.* The M-**fcu**-MOF crystals were dried in a vacuum oven at 175 ^{o}C for 12 h, then a designated amount of crystals was dispersed in THF solution to form 15 wt% M-**fcu**-MOF/THF suspension. The M-**fcu**-MOF/THF suspensions were then added to 15 wt% 6FDA-polyimide/THF solution to form dopes. After being mixed thoroughly on a rolling mixer overnight, excess solvent in the dope was removed by purging the dope slowly using dry nitrogen. M-**fcu**-MOF/6FDA-polyimide hybrid dense films with designated MOF loading were then formed using a same casting procedure as preparing pure 6FDA-polyimide dense films.

Characterization of Materials. The dense films for scanning electron microscope (SEM, Hitachi, SU8010) test were prepared by first soaking films in hexane and then cryogenically fracturing in liquid nitrogen to preserve their microstructures. Wide-angle X-ray diffraction (WAXD) was measured on a Panalytical Empyrean diffractometer operating with a Cu Kα radiation at a wavelength of 1.54 Å, in a 2θ range of 5 - 50°. Glass transition of polymers were measured using Q600 with simultaneous measurement of weight change (TGA, thermalgravimetric analysis) and true differential heat flow (DSC, differential scanning calorimetry) on the same sample under continuous N_2 purging. The samples first preheated to 150 ^oC for 1 hr before measuring the glass transition properties.

Pure Gas Sorption Tests. Gas sorption isotherms at pressure up to ~8 bar at 308 K were measured using a pressure decay method. All samples were activated at 175 °C under vacuum for 24 h and then loaded into cell (B) and degassed for overnight. A differential amount of sorption gas was first introduced into the reservoir (A), then the connecting valve was quickly open for 1 second and closed. The pressure signal in both volume (A) and volume (B) were recorded continuously. Detailed descriptions of the pressure decay method can be found elsewhere.

Gas permeation Tests. The gas permeation was conducted in a variable pressure, constant-volume apparatus. Pure gas permeation tests were performed at 1.4 bar, 1.4 bar and 4.2 bar for H_2S, CO_2 and CH_4, respectively and 308 K. Mixed gas permeation tests were performed using three $H_2S/CO_2/CH_4$ gas mixtures in different $H_2S/CO_2/CH_4$ compositions, i.e. 20/20/60, 25/5/70, and 0.5/20/79.5, respectively, at pressures up to ~56 bar. The downstream composition was determined using a gas chromatograph (Varian 450-GC). The stage cut (the flow rate ratio of

permeate to feed) was maintained between 1% - 5% to avoid concentration polarization on the upstream side of the permeation cell, keeping the driving force across the membrane constant throughout the course of the experiment. All membranes were pre-saturated under the target pressure for 1 to 6 hours, depending on the material and pressure used to ensure that all mixed gas data were collected at *steady state*. The overall downstream pressure changing with time (*dp*/*dt*) and the product gas composition were monitored continuously in the process. The final data were collected by averaging the stabilized data points, usually 2-3 points with negligible variation from each other. Finally, the vented exhaust H_2S containing gas mixture were saturated with NaOH solution to avoid potential environmental issues.

Permeability, Solubility, Diffusivity and Energetic Factors. Permeability and selectivity were used to characterize the membrane separation performance. The permeability, P_i, describes the intrinsic gas separation productivity of a dense film membrane and is defined by the flux of penetrant *i*, n_i, normalized by the membrane thickness, *l*, and the partial pressure or fugacity difference, Δf_i, across the membrane, viz.,

$$P_i = \frac{n_i \cdot l}{\Delta f_i} \quad \text{(Eq. 1)}$$

In order to estimate pure gas permeability, the slope of the permeate pressure vs. time (*dp/dt*); membrane thickness (*l*); downstream volume (*V*); operating temperature (*T*); and transmembrane pressure or fugacity difference (Δf) were used:

$$P = \frac{\frac{dp}{dt} \cdot l \cdot V}{A \cdot T \cdot \Delta f} \quad \text{(Eq. 2)}$$

The mixed gas permeability coefficient of component *i* (P_i) is calculated using its molar fraction in the permeate (x_i) and the transmembrane fugacity difference (Δp_i):

$$P_i = \frac{\frac{dp}{dt} \cdot x_i \cdot l \cdot V}{A \cdot T \cdot \Delta f_i} \quad \text{(Eq. 3)}$$

As note in Eq. 3, in the permeation calculation, fugacity (NIST software standard reference database) was used instead of partial pressure to account for the non-idealities of gases. The perm-selectivity, α_{ij}, is determined by the ratio of the component *i* permeability to the component *j* permeability:

$$\alpha_{ij} = \frac{P_i}{P_j} \quad \text{(Eq. 4)}$$

Permeability can also be expressed as the product of the average effective diffusion coefficient (*D*) and sorption coefficient (*$*) of a given gas *i* within the membrane:

$$P_i = D_i \cdot \$_i \quad \text{(Eq. 5)}$$

The sorption coefficient represents the thermodynamic contribution to transport, which can be measured independently by pressure-decay sorption. The sorption coefficient can be expressed as:

$$\$_i = \frac{c_i}{f_i} \quad \text{(Eq. 6)}$$

where c_i is the concentration of a gas adsorbed in the sample, and f_i is the corresponding upstream fugacity driving force of component *i*. In this work, the adsorbed gas concentration in films was described by the dual-mode sorption model, which is given as:

$$c_i = c_{D,i} + c_{H,i} = k_{D,i} \cdot f_i + \frac{C'_{H,i} \cdot b_i \cdot f_i}{1 + b_i \cdot f_i} \quad \text{(Eq. 7)}$$

where $c_{D,i}$ is the Henry's law or dissolved mode penetrant concentration, $c_{H,i}$ is the penetrant concentration in the Langmuir mode or hole-filling sorption mode. The $k_{D,i}$ is the Henry's law sorption coefficient reflecting properties of polymer matrix. On the other hand, $C'_{H,i}$ is the Langmuir capacity constant, and b_i is the Langmuir affinity constant, which reflect the average

of these parameters contributed by the glassy polymer and MOF. Sorption results of MMMs, i.e. Y-*fum*-**fcu**-MOF/6FDA-DAM are available in previous study [30].

The effective diffusion coefficient (*D*) in the membrane was calculated from the independently measured permeability (*P*) and sorption coefficient (*S*):

$$D_i = \frac{P_i}{\$_i} \quad \text{(Eq. 8)}$$

Maxwell Back-calculations. The Maxwell model is used to mathematically describe the gas transport in mixed-matrix materials and to back-calculate permeability in dispersed molecular sieve particles. Maxwell model is given by:

$$P_{MMM} = P_p \left[\frac{P_s+2P_p-2\emptyset_s\cdot(P_p-P_s)}{P_s+2P_p+\emptyset_s\cdot(P_p-P_s)}\right] \quad \text{(Eq. 9)}$$

where P_{MMM} is permeability in the mixed matrix material; P_p is permeability in the polymer matrix; P_S is permeability in dispersed molecular sieve particles; and ϕ_s is volume fraction of molecular sieve particles in the mixed matrix material.

The permeability of pure M-**fcu**-MOF membrane is calculated using the following equation:

$$P_S = P_P \left[\frac{2P_M-2P_P+\emptyset_S\cdot(2P_p+P_M)}{P_P-P_M+\emptyset_S\cdot(2P_p+P_M)}\right] \quad \text{(Eq. 10)}$$

The diffusion coefficient in the MOF at steady state can be obtained using Eq. 8 after obtained the sorption coefficient in the MOF by gas sorption tests.

Density functional theory (DFT) calculations [31]. The Becke exchange plus Lee-Yang-Parr correction (BLYP) exchange-correlation functional with double numeric polarization (DNP) basis set was used in all the calculations. DFT semicore pseudopots (DSPP), which is developed specifically for DMol^3 calculations, was used to set the type of core treatment[40]. A real-space orbital global cutoff of 4.0 Å was applied, and the convergence threshold parameters for the

optimization were 2×10^{-5} (energy), 4×10^{-3} (gradient), and 5×10^{-3} (displacement), respectively. Grimme method for DFT-D approach was used to further improve the accuracy.

Results

Tuning gas sorption and diffusion properties by tailorable MOF chemistry

We chose M-**fcu**-MOFs (M = metal; **fcu** = face-centered cubic) [32] as advanced fillers in the polymer matrices primarily due to their extraordinary stability under aggressive H_2S conditions [28,33,34] as well as excellent structural tunability [27]. The M-**fcu**-MOFs comprise molecular building blocks (MBBs) that are 12-fold connected to adjacent MBBs through various organic linkers, forming a highly connected **fcu** topology. Both the inorganic MBBs and the organic linkers can be modulated independently [35], introducing diverse functionalities and pore-apertures for tuning gas permeation properties. For instance, Figure 2a shows the crystalline structure of Zr-*fum*-**fcu**-MOF enclosing two types of cages, i.e. tetrahedral (purple) and octahedral (yellow), whose faces comprise one type of triangular window as the sole entrance to the inner pore system [27,36,37]. By substituting the metal, i.e. $Zr^{4+} \rightarrow Y^{3+}$, and the organic linkers, i.e. fumarate (*fum*) and methylfumarate (*mfum*), the pore-aperture sizes are rationally tuned to exploit different guest molecules (Figure 2b) [27,30]. Moreover, the MBBs of Zr-*fum*-**fcu**-MOF and Zr-*mfum*-**fcu**-MOF contain μ_3-OH groups that alternatively bind to Zr_6-octahedral clusters [36], which is absent in the Y-*fum*-**fcu**-MOF (Figure S4) [32]. However, unlike the exposed μ_3-OH groups approachable for binding adsorbates in the Zr-*fum*-**fcu**-MOF (Figure S3), the μ_3-OH groups in the Zr-*mfum*-**fcu**-MOF are only partially shielded by the $-CH_3$ groups on the organic likers along with cage size reductions (Figure S5), thereby increasing the activation energies of diffusion for H_2S, but not CH_4. Additionally, the bulky $-CH_3$ groups on the linkers

also introduce reduced size and irregular shape of the pore-aperture, which may affect the gas diffusion behaviors of Zr-*mfum*-**fcu**-MOF. In any case, the complex interplay of such effects, still allows creating a tailorable M-**fcu**-MOF platform with diverse functionalities and pore-apertures for tuning gas separation performances.

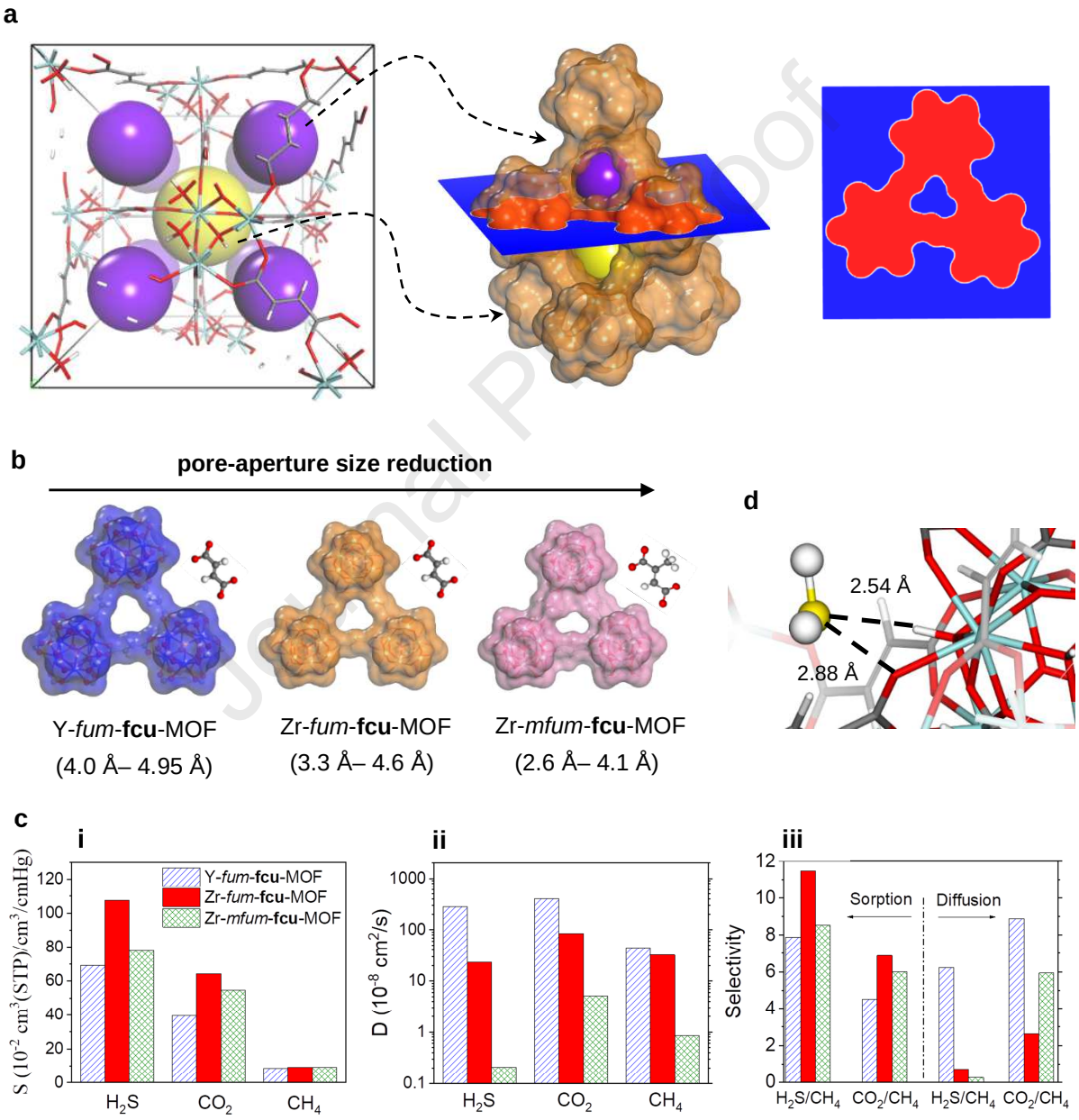

Figure 2. Designated M-fcu-MOF platform for $H_2S/CO_2/CH_4$ separation. (a) A unit cell of Zr-*fum*-**fcu**-MOFs (left) encloses the tetrahedral cage (purple) and octahedral cage (yellow). The two types of cages (middle) are interconnected by a triangular pore-aperture (right). (b) Pore-apertures of M-**fcu**-MOFs represented by the van der Waals (vdW) surface using Connolly Radius [38]. Notably, the free rotations of the -CH_3 functional groups about the C-C single bonds in Zr-*mfum*-**fcu**-MOF can also affect the effective pore-aperture size. More descriptions are available in Figure S3 - S6. (c) gas sorption (i), diffusion (ii) coefficients and selectivities (iii) of the M-**fcu**-MOFs measured at 35 ^oC and 1.38 bar (H_2S), 1.38 bar (CO_2) and 4.14 bar (CH_4), respectively. (d) Preferential sorption configuration of an H_2S molecule interacting with the μ_3-OH functional group in Zr-*fum*-**fcu**-MOF by density functional theory (DFT) calculations. Details and more information are available in the Methods and Supplementary Information.

By tailoring the MOF chemistry, the H_2S, CO_2 and CH_4 sorption and diffusion coefficients of the M-**fcu**-MOFs can be rationally tuned, as shown in Figure 2c. Specifically, Zr-*fum*-**fcu**-MOF exhibits more attractive H_2S and CO_2 sorption advantages over Y-*fum*-**fcu**-MOF and Zr-*mfum*-**fcu**-MOF, whereas all three MOFs show comparative CH_4 sorption abilities (Figure 2c-i and Figure S10). On the other hand, the gas diffusion properties of the M-**fcu**-MOFs show a different trend (Figure 2c-ii), i.e. Y-*fum*-**fcu**-MOF > Zr-*fum*-**fcu**-MOF > Zr-*mfum*-**fcu**-MOF, agreeing well with the reduction of the pore-aperture sizes (Figure 2b). As a result, Zr-*fum*-**fcu**-MOF and Y-*fum*-**fcu**-MOF show the best sorption and diffusion tradeoffs, respectively, for H_2S/CH_4 and CO_2/CH_4 separations (Figure 2c-iii). Clearly, therefore, we have created a tailorable M-**fcu**-MOF platform that tunes the gas transport behaviors through different fundamentals, i.e. sorption vs. diffusion.

We further explored the exceptional H_2S sorption favorability of Zr-*fum*-**fcu**-MOF, which is mainly attributed to its exposed μ_3-OH functional groups. Density functional theory (DFT)

calculations reveal that the μ_3-OH group is the preferential H_2S sorption site in the Zr-*fum*-**fcu**-MOF with a remarkable interaction energy of -72.5 kJ/mol (Figure 2d). This strongly negative interaction is significantly higher than the highest H_2S interaction energy in the Y-*fum*-**fcu**-MOF without the μ_3-OH groups (Table S1). On the other hand, the μ_3-OH groups in the Zr-*mfum*-**fcu**-MOF are geometrically shielded by $-CH_3$ groups on the organic likers, reducing H_2S interaction strength (Table S1). The same trend is also explored for CO_2 adsorption in the M-**fcu**-MOFs, whereas the CH_4 adsorption is negligibly affected. Overall, H_2S is highly sorption-competitive over CO_2 and CH_4 in the M-**fcu**-MOFs, especially in the Zr-*fum*-**fcu**-MOF.

Controlling penetrate competition using selected MOF fillers

To pursue the larger mixed matrix vision outlined above, we next investigated the effects of incorporating different M-**fcu**-MOF fillers into a specific high performing polyimide by solution-casting to form dense film membranes (Methods). Here, we chose the 6FDA(4,4'-(hexafluoroisopropylidene)dipphthalic anhydride)-DAM(DAM: 2,4-Diaminomesitylene) polyimide as starting material for screening MOF fillers. This polyimide has already been shown to be easily formed into a thin-skinned composite hollow fiber with the MOF only in the skin layer [25]. Various spinnable polyimide matrices will be discussed later. In the current work, only "simple" dense flat film samples are considered here to avoid the need to optimize spinning until a preferred MOF/polymer pair is selected. The MOF crystals were uniformly dispersed in the polymer matrix with requisite excellent MOF/polymer interface compatibility (Figure S8), which is further supported by the permeation results as discussed in following sections. Indeed, previous studies have revealed strong hydrogen bonding between *fcu*-MOFs and 6FDA-based

polyimides [39,40]. The developed M-**fcu**-MOF/6FDA-DAM hybrid membranes with different MOF loading amounts, i.e. 10 wt% (**1**) and 20 wt% (**2**), were measured under pure gas and $H_2S/CO_2/CH_4$ ternary mixed gas (20/20/60 in molar) conditions at 35 ^oC and 6.9 bar (Methods).

Notably, all three kinds of M-**fcu**-MOF/6FDA-DAM hybrid membranes show different trends between pure gas results and mixed gas results (Figure 3a). For instance, pure gas permeation results suggest negligible enhancements for either H_2S/CH_4 or CO_2/CH_4 separation by the Zr-*fum*-**fcu**-MOF incorporated hybrid membranes; however, the mixed gas measurements reveal a remarkable simultaneous enhancement for both separations. This suggests excellently tuned molecular competitions among H_2S, CO_2 and CH_4 in the mixed gas permeation process through the Zr-*fum*-**fcu**-MOF fillers. Indeed, this claim is further supported by the Zr-*mfum*-**fcu**-MOF/6FDA-DAM membrane and Y-*fum*-**fcu**-MOF/6FDA-DAM membrane results (Figure 3a). Nevertheless, Zr-*fum*-**fcu**-MOF outperforms the other M-**fcu**-MOFs on both H_2S/CH_4 and CO_2/CH_4 separations, indicating the uniqueness of its sorption and/or diffusion properties on controlling the molecular competitions.

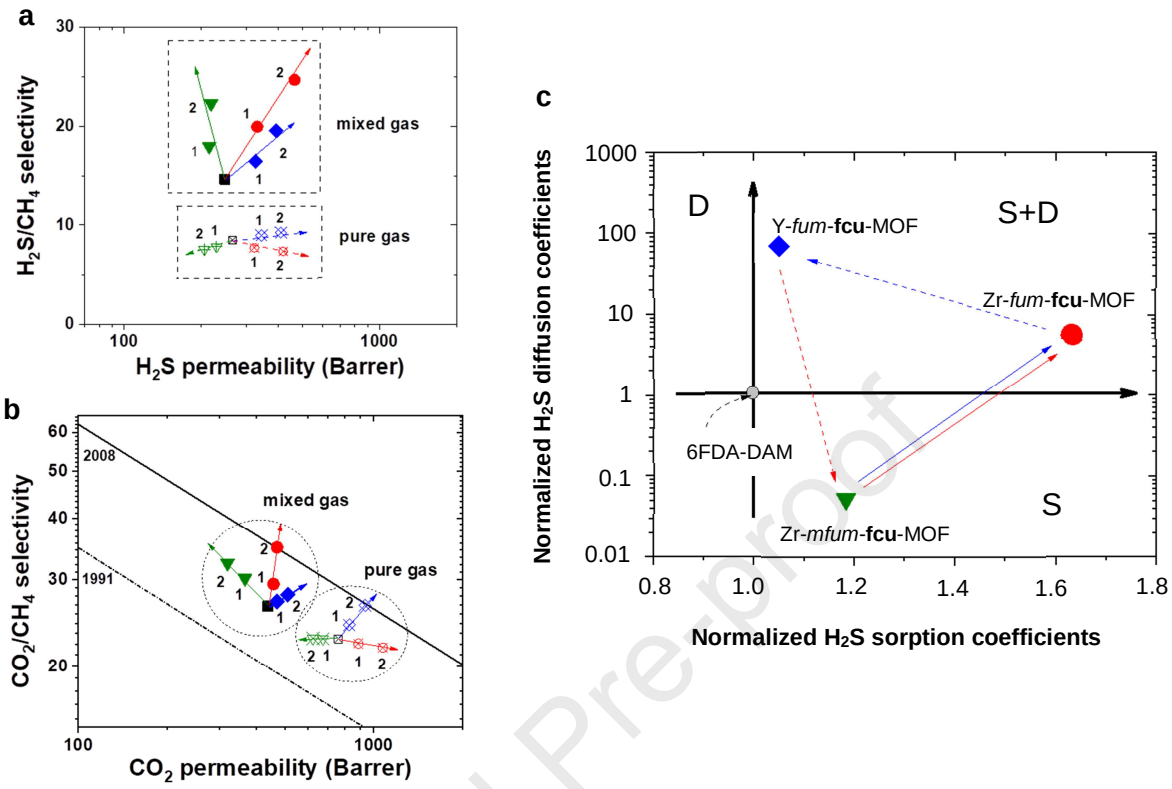

Figure 3. Promoted membrane separation performance by MOF-controlled penetrate competition. (a) H_2S/CH_4 and (b) CO_2/CH_4 separation performance of the hybrid membranes developed by incorporating different M-**fcu**-MOFs, i.e. Y-*fum*-**fcu**-MOF (blue diamond), Zr-*fum*-**fcu**-MOF (red circle) and Zr-*mfum*-**fcu**-MOF (green triangular), into the same 6FDA-DAM polyimide (black square). The MOF loading amounts are designed to 10 wt% (**1**) and 20 wt% (**2**) in the hybrid membranes. The pure gas (open) and ternary mixed gas (solid) permeation measurements were performed at 35 ^oC with H_2S, CO_2, and CH_4 fugacity of 1.38 bar, 1.38 bar and 4.14 bar, respectively. The Robeson upper bounds for CO_2/CH_4 binary gas separation using polymer membranes are shown for comparison. (c) Normalized H_2S sorption and diffusion coefficients of M-**fcu**-MOFs using the 6FDA-DAM polyimide results.

The competitive-permeation strengths among H_2S, CO_2 and CH_4 can be quantified by comparing the mixed gas permeation results with the pure gas results. For instance, mixed gas

results indicate that the CH_4 permeation is inhibited by the incorporated Zr-*fum*-**fcu**-MOF fillers in 6FDA-DAM, which is different from the dramatic enhancement observed in the pure gas results (Figure S11). This discrepancy is attributed to the weakest competitive-permeation strength of CH_4 in comparison with H_2S and CO_2. Indeed, the incorporated Zr-*fum*-**fcu**-MOF fillers greatly promote the H_2S permeation in the membranes (Figure 3a) while slightly increasing CO_2 permeation (Figure 3b). Ultimately, the CH_4 molecules are "beaten" by the H_2S and CO_2 molecules in the permeation process due to tuned molecular competitions introduced by the Zr-*fum*-**fcu**-MOF incorporation. Although the Y-*fum*-**fcu**-MOF or Zr-*mfum*-**fcu**-MOF fillers also affect the molecular transport in the hybrid membranes (Figure S12 and S13), the molecular competitions among H_2S, CO_2 and CH_4 are not as precisely controlled as those in Zr-*fum*-**fcu**-MOF fillers (Figure S11). This is because *the H_2S sorption favorability of the MOF dominates the overall molecular competitions among H_2S, CO_2 and CH_4.*

To further illustrate the significance of H_2S sorption favorability on controlling the membrane performance, we normalized the H_2S sorption and diffusion coefficients of the M-**fcu**-MOFs using the 6FDA-DAM results (Figure 3c). The enhanced H_2S sorption advantage from the incorporated M-**fcu**-MOF fillers promotes the H_2S/CH_4 and CO_2/CH_4 selectivities of the polyimide membrane (Figure 3a and 3b). The H_2S diffusion coefficients only affect the H_2S permeability of the membranes. Therefore, the Zr-*fum*-**fcu**-MOF with the most favorable H_2S sorption advantage but a negligible H_2S diffusion advantage performs the best in H_2S/CH_4 separation. Notably, the tailored H_2S sorption in MOFs can also promote the CO_2 sorption in mixed gas conditions, advantaging the CO_2/CH_4 separation. Our DFT calculations reveal that the highest CO_2 interaction energy in Zr-*fum*-**fcu**-MOF is promoted by 11% (-53.2 kJ/mol → -59.0 kJ/mol) due to pre-sorption of a H_2S molecule in the framework. In this regard, the enhanced

CO_2 sorption can further improve the competitive strength of CO_2 over CH_4, resulting in the different trends for CO_2/CH_4 selectivity in mixed gas vs. pure gas measurements in Figure 3b. This is outstanding, since the complex ternary mixture permeation process through a hybrid membrane is significantly simplified with only one dominating factor, i.e. H_2S sorption ability in MOFs.

Membrane tunability by polymer chemistry

Beside the dramatic role of MOF fillers on enhancing gas separation efficiencies, polymer matrices usually provide an advanced platform for tuning permeability and selectivity based on the permeability-selectivity trade-off of polymer membranes [41]. Obviously, such a trade-off relationship is essential to MOF/polymer hybrid membrane developments for $H_2S/CO_2/CH_4$ separation, allowing to fine-tune the permeabilities of H_2S and CO_2 as well as selectivities of H_2S/CH_4 and CO_2/CH_4 to meet diverse separation requirements. Unfortunately, compared to the widely studied CO_2/CH_4 separation, the trade-off relationship of H_2S/CH_4 separation is much less revealed and understood. We therefore tailored the 6FDA-polyimide backbone (Figure 4a) to explore the permeability vs. selectivity tradeoff (Figure 4b and c). However, our initial effort on choosing crosslinkable 6FDA-DAM/DABA_3:2 (DABA: 3,5-diaminobenzoic) as matrix introduce unappealing H_2S/CH_4 separation performance (Figure 4b), though its CO_2/CH_4 separation performance remains reasonably good (Figure 4c). This is attributed to the fact that the carboxyl groups form strong hydrogen bonds among themselves, reducing sorption affinity and free volume for H_2S sorption [16]. Incorporated MOF fillers can promote the H_2S/CH_4 separation efficiencies in hybrid membranes, whereas the overall performance cannot compete with 6FDA-DAM-based membranes due to significantly low H_2S permeability (Figure 4b).

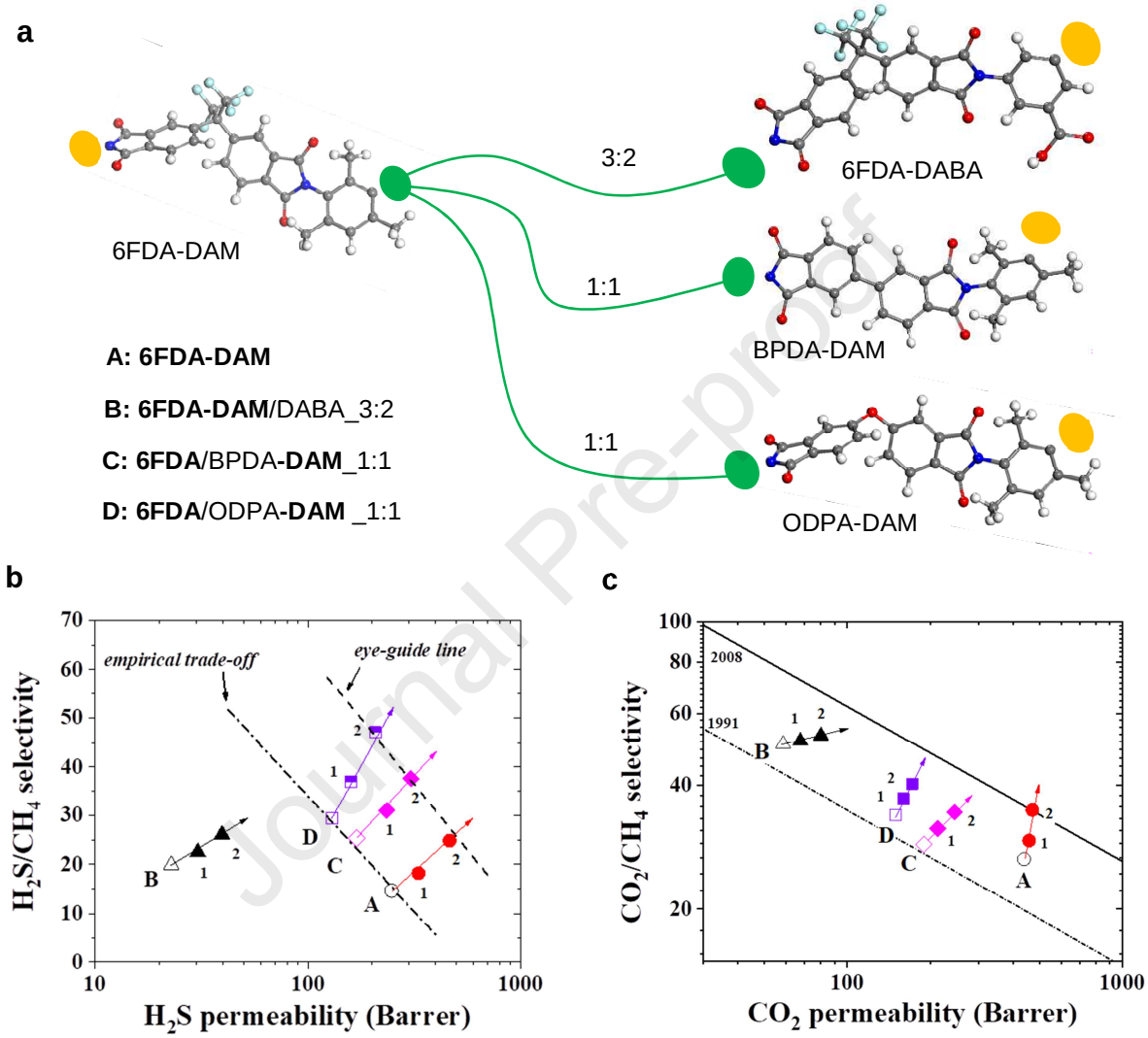

Figure 4. Membrane tunability by tailoring the polymer chemistry. (a) Chemical structures of 6FDA-polyimides tuned by combining different moieties in different ratios. The 6FDA-polyimides are formed by repeated polymer chains, while the linking points on the moieties are illustrated in colored ellipses. Detailed structures are available in Figure S2. Atoms in the structures: C (gray), N (blue), O (red), F (cyan) and H (white). (b) H_2S/CH_4 and (c) CO_2/CH_4 separation performance of hybrid membranes derived by incorporating the Zr-*fum*-**fcu**-MOF fillers into

the 6FDA-polyimides in comparison with pure 6FDA-polyimide membranes. All data were measured using an $H_2S/CO_2/CH_4$ (20/20/60 in molar) ternary mixture at 35 ^oC and 6.9 bar.

In this regard, we investigated two new 6FDA-polyimides, 6FDA/BPDA-DAM_1:1 (BPDA: 3:3',4,4'-biphenyl dianhydride) and 6FDA/ODPA-DAM_1:1 (ODPA: 4,4'oxydiphthalic anhydride), without strong interchain interactions for prohibiting over-condensed packing of the polymer (Figure 4a). Compared to 6FDA-DAM, BPDA-DAM and ODPA-DAM exhibit more condensed chain packing due to the partially (1/2) substitution of the bulky $-CF_3$ groups. Moreover, the rotatable ether group (-O-) in ODPA-DAM results in better chain packing ability in comparison with the rigid BPDA-DAM. Overall, the fine-tune of the polyimide backbones introduces enhanced chain packing in order of ODPA > BPDA-DAM > 6FDA-DAM. Promisingly, attractive permeability vs. selectivity tradeoff for H_2S/CH_4 separation is observed, surpassing the performance restriction induced by crosslinking in the 6FDA-DAM/DABA_3:2 membrane (Figure 4b). Finally, the incorporation of Zr-*fum*-**fcu**-MOF fillers into the uncrosslinkable 6FDA-polyimides further promote both H_2S/CH_4 and CO_2/CH_4 separations (Figure 4b and 4c), pushing the trade-off relationship to more attractive regions for the separation. This feature is important for balancing the permeability vs. selectivity in practical applications, which will be discussed in the following sections.

MOF-controlled plasticization benefits

The fabricated MOF/polymer hybrid membranes were eventually investigated under aggressive natural gas sweetening conditions to explore their potentials in realistic applications.

Promisingly, compared to pure polymer membranes, MOF incorporation changes the plasticization response of the polyimides, allowing controlled plasticization benefits. Here we show an example of MOF-polymer hybrid membrane, i.e. Zr-*fum*-**fcu**-MOF/6FDA-ODPA-DAM_10wt%, measured using an $H_2S/CO_2/CH_4$ (20/20/60) ternary gas mixture at 308 K with pressures up to 56 bar (solid lines, Figure 5a and 5b). The results of a pure 6FDA/ODPA-DAM polyimide membrane are also shown for comparison (dashed lines). Generally, the pristine 6FDA/ODPA -DAM polyimide membrane shows a typical plasticization benefit, as evidenced by the promoted H_2S permeability and H_2S/CH_4 selectivity under high pressures. However, a limit of the H_2S/CH_4 selectivity is shown above ~40 bar due to *over*-plasticization as also observed in other glassy polymer membranes [16,18]. Remarkably, this selectivity limit is successfully overcome by incorporating Zr-*fum*-**fcu**-MOF fillers into the polymer (Figure 5b). In comparison with the pure polyimide membrane, we achieve a continuous increase of the H_2S/CH_4 selectivity and a significant enhancement of the CO_2/CH_4 selectivity using the MOF-polymer hybrid membrane with the increase of pressure up to 56 bar (Figure 5b). On the other hand, controlled plasticization still promotes H_2S and CO_2 permeabilities under high pressures (Figure 5a). As results, the Zr-*fum*-**fcu**-MOF/6FDA-ODPA-DAM _10wt% membrane exhibits a $S_{H2S/CH4} \approx 63$ and a $S_{CO2/CH4} \approx 26$ as well as a $P_{H2S} \approx 360$ barrer and a $P_{CO2} \approx 160$ barrer at 56 bar, surpassing the (H_2S+CO_2) simultaneous removal target.

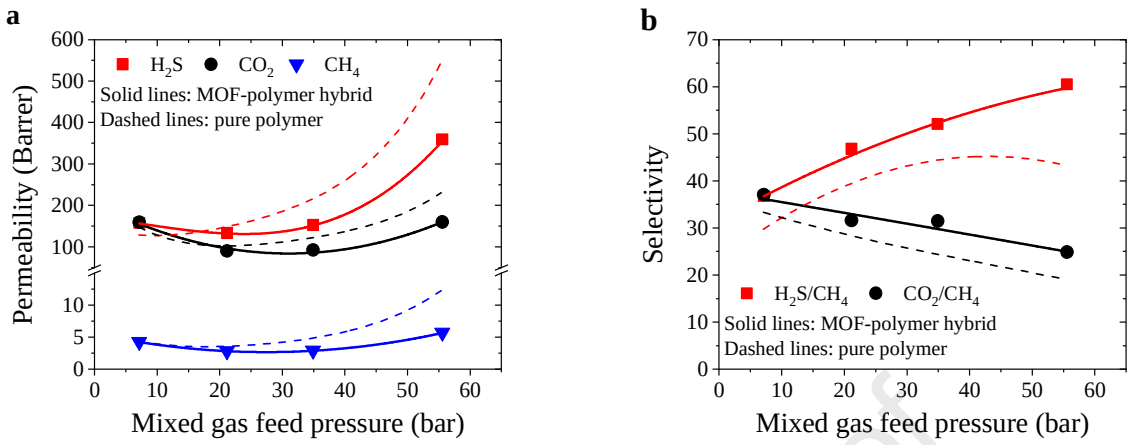

Figure 5. Plasticization responses of MOF-polymer hybrid membranes. Comparison of (a) H_2S, CO_2 and CH_4 permeabilities, and (b) H_2S/CH_4 and CO_2/CH_4 selectivities between a Zr-*fum*-**fcu**-MOF/6FDA-ODPA-DAM _10wt% hybrid membrane (solid lines) and a pure 6FDA/ODPA-DAM membrane (dashed lines) using an $H_2S/CO_2/CH_4$ (20/20/60) ternary mixture measured at 35 ^oC.

Thanks to the MOF-controlled plasticization benefits, the (H_2S+CO_2) simultaneous removal target is also achieved in other Zr-*fum*-**fcu**-MOF/6FDA-polyimide hybrid membranes with MOF loading amounts ranging from 10 wt% to 20 wt% (Figure S15 - S17). These facts show that incorporating rigid MOF fillers is a powerful tool to tune natural gas sweetening performance of polyimide membranes by stabilizing the soft polymer chains., demonstrating the proposed *MOF-controlled plasticization benefits* in Figure 1. Furthermore, the Zr-*fum*-**fcu**-MOF fillers also control the plasticization benefits under various $H_2S/CO_2/CH_4$ ternary gas compositions with H_2S concentrations ranging from 0.5% to 25% (Figure S18 - Figure S21). Indeed, varying ternary gas compositions affect the plasticization responses of the hybrid membrane, whereas the undesired *over*-plasticization is overcome in all conditions. This

noteworthy fact demonstrates that the MOF-polymer hybrid membranes can be applied in various (H_2S+CO_2) simultaneous removal applications.

Tunable MOF-polymer hybrid membrane platform for capturing H_2S and CO_2

We hereby summarize the $H_2S/CO_2/CH_4$ separation performances of the rationally designed Zr-*fum*-**fcu**-MOF-polyimide hybrid membranes at 56 bar under various gas compositions in Figure 6. Generally, the developed hybrid membranes show extraordinary H_2S/CH_4 and CO_2/CH_4 separation efficiencies at 56 bar, surpassing the empirical tradeoff relationships for polymer membranes under high pressures (> 30 bar). Moreover, the hybrid membrane performances are highly tunable in terms of permeability vs. selectivity by choosing different polymer matrices while preserving the attractive H_2S and CO_2 simultaneous removal feature. In this regard, we built a tunable membrane platform fulfilling the diverse natural gas sweetening requirements.

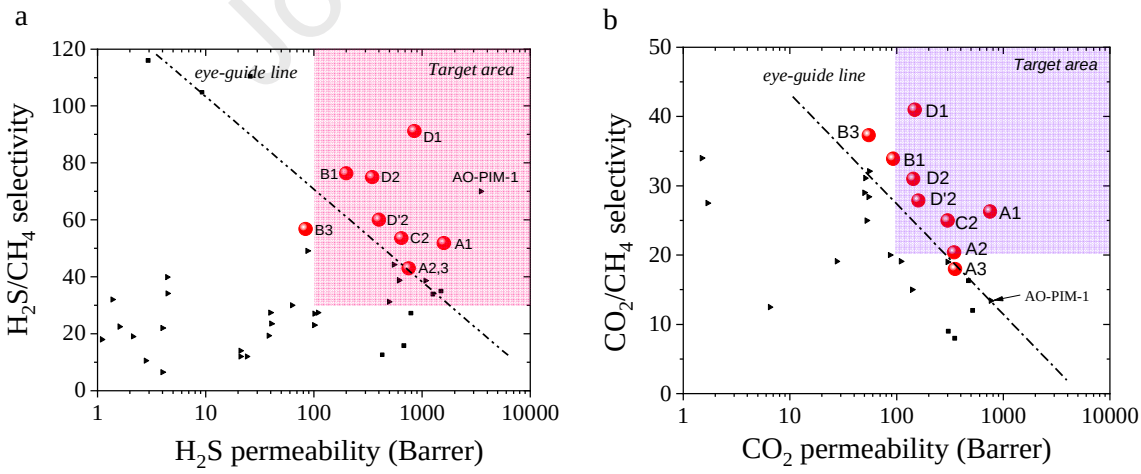

Figure 6. Tunable MOF-polymer hybrid membrane performances under realistic conditions. (a) H_2S/CH_4 separation, and (b) CO_2/CH_4 separation. The colored boxes represent the (H_2S+CO_2) simultaneous removal target for a single membrane device. The eye-guide lines represent empirical tradeoff relationships for H_2S/CH_4 and CO_2/CH_4 separations based on rubbery (solid black square) and glassy (solid black triangle) polymer membrane data obtained using $H_2S/CO_2/CH_4$ ternary mixtures under various temperatures and high feed pressures (> 30 bar) shown in Table S3. The hybrid membranes are based on the recipe of Zr-*fum*-**fcu**-MOF filler and different 6FDA-polyimides (**A**, **B**, **C** and **D**, as shown in Figure 4a, with 20 wt% MOF loading amount, while **D'** represents 10 wt% MOF loading). A: 6FDA-DAM, B: 6FDA-DAM/DABA_3:2, C: 6FDA/BPDA-DAM_1:1 and D: 6FDA/ODPA-DAM_1:1. The membranes were measured under various $H_2S/CO_2/CH_4$ compositions, i.e. 0.5/20/79.5 (**1**), 20/20/60 (**2**), and 25/5/70 (**3**) at 35 ^oC and 56 bar. Data are available in Table S4.

In the past, rubbery polymer membranes were considered as better choices for the sorption dominated H_2S/CH_4 separation [1]. However, the developed MOF-polymer hybrid membranes outperform the reported rubbery polymer membranes for H_2S/CH_4 separation (Figure 6a) with the extra benefits of providing much higher CO_2/CH_4 separation efficiency (Figure 6b). Moreover, the hybrid membranes also show comparable H_2S/CH_4 separation performance with the high-performing AO-PIM-1 [18] glassy polymer membrane but exhibit much higher CO_2/CH_4 separation performance. Comparing with current commercial membrane materials for H_2S/CH_4 separation (ether-amide block co-polymer) and CO_2/CH_4 separation (cellulose acetate, etc.) [1], the MOF-polymer hybrid membranes exhibit much higher performance for both separations. Finally, considering *the highly spinnable feature of the hybrid materials* derived based on the 6FDA-polyimides [25,42], more attractive membrane performances are expected by translating the developed MOF-polymer hybrid recipes to asymmetric hollow fiber membranes in further studies.

Conclusions

In summary, we rationally built a highly tunable MOF-polyimide hybrid membrane platform that dramatically outperforms current membranes for (H_2S+CO_2) simultaneous removal under realistic application conditions. The hybrid formulation combining the MOF chemistry and the polymer chemistry introduces tailorable H_2S/CH_4 and CO_2/CH_4 separation performances, meeting the diverse separation requirements between different natural gas reservoirs around the world. Moreover, the hybrid approach by incorporating rigid MOF fillers into soft polyimides controls the plasticization responses of the polyimide as well as the molecular competitions among H_2S, CO_2 and CH_4. This work suggests that the future natural gas sweetening market can be revolutionized by designed high-efficiency MOF-polymer hybrid membranes, a more economical solution for treating H_2S and CO_2. Future efforts will focus on producing thin hybrid membranes toward real application in natural gas sweetening.

Acknowledgments

The research supported in this publication was supported by DOE BES grant (DE-FG02-04ER15510) and KAUST CRG Research Grant URF/1/222-01. Y.L., W.Q., G.L., and W.J.K. acknowledge the support by the Roberto C. Goizueta Chair fund and the Specialty Separations Center at Georgia Institute of Technology for assistance in equipment resource funds.

Appendix A. Supplementary Information

Supplementary data associated with this article can be found in the online version.

References

[1] R. W. Baker, K. Lokhandwala, Natural Gas Processing with Membranes: An Overview, Ind. & Eng. Chem. Res., 47 (2008) 2109-2121.

[2] M. S. Shah, M. Tsapatsis, J. I. Siepmann, Hydrogen Sulfide Capture: From Absorption in Polar Liquids to Oxide, Zeolite, and Metal-Organic Framework Adsorbents and Membranes, Chem. Rev. 117 (2017) 9755-9803.

[3] A. Hayek, A. Alsamah, N. Alaslai, H. Maab, E. A. Qasem, R. H. Alhajry, N. M. Alyami, Unprecedented Sour Mixed-Gas Permeation Properties of Fluorinated Polyazole-based Membranes, ACS Appl. Polym. Mater., 2 (2020) 2199-2210.

[4] Y. Belmabkhout, P. M. Bhatt, K. Adil, R. S. Pillai, A. Cadiau, A. Shkurenko, G. Maurin, G. Liu, W. J. Koros, M. Eddaoudi, Natural Gas Upgrading using a Fluorinated MOF with Tuned H_2S and CO_2 Adsorption Selectivity, Nat. Energy, 3 (2018) 1059-1066.

[5] A.D. Wiheeb, I. K. Shamsudin, M. A. Ahmad, M. N. Murat, J. Kim, M. R. Othman, Present Technologies for Hydrogen Sulfide Removal from Gaseous Mixtures, Rev. Chem. Eng., 29 (2013) 449-470.

[6] H. B. Park, J. Kamcev, L. M. Robeson, M. Elimelech, B. D. Freeman, Maximizing the Right Stuff: The Trade-Off between Membrane Permeability and Selectivity, Science, 356 (2017).

[7] K. Dalane, Z. D. Dai, G. Mogseth, M. Hillestad, L. Y. Deng, Potential Applications of Membrane Separation for Subsea Natural Gas Processing: A Review, J. Nat. Gas Sci. Eng., 39 (2017) 101-117.

[8] R. P. Lively, D. S. Sholl, From Water to Organics in Membrane Separations, Nat. Mater., 16 (2017) 276-279.

[9] J. Hennessy, A. Livingston, R. Baker, Membranes from Academia to Industry, Nat. Mater., 16 (2017) 280-282.

[10] W. J. Koros, C. Zhang, Materials for Next-Generation Molecularly Selective Synthetic Membranes, Nat. Mater., 16 (2017) 289-297.

[11] Y. S. Lin, Inorganic Membranes for Process Intensification: Challenges and Perspective, Ind. Eng. Chem. Res. 58 (2019) 5787-5796.

[12] D.J. Harrigan, J. A. Lawrence, H. W. Reid, J. B. Rivers, J. T. O'Brien, S. A. Sharber, B. J. Sundell, Tunable Sour Gas Separations: Simultaneous H_2S and CO_2 Removal from Natural Gas via Crosslinked Telechelic Poly(Ethylene Glycol) Membranes, J. Membr. Sci., 602 (2020) 117947.

[13] A. A. Alghannam, G. O. Yahaya, A. Hayek, I. Mokhtari, Q. Saleem, D. A. Sewdan, A. A. Bahamdan, High Pressure Pure- and Mixed Sour Gas Transport Properties of Cardo-Type Block Co-Polyimide Membranes, J. Membr. Sci., 553 (2018) 32-42.

[14] T. Visser, G. Koops, M. Wessling, On the Subtle Balance between Competitive Sorption and Plasticization Effects in Asymmetric Hollow Fiber Gas Separation Membranes, J. Membr. Sci., 252 (2005) 265-277.

[15] J. T. Vaughn, W. J. Koros, Analysis of Feed Stream Acid Gas Concentration Effects on the Transport Properties and Separation Performance of Polymeric Membranes for Natural Gas Sweetening: A Comparison between a Glassy and Rubbery Polymer, J. Membr. Sci., 465 (2014) 107-116.
[16] Y. Liu, Z. Liu, G. Liu, W. Qiu, N. Bhuwania, D. Chinn, W. J. Koros, Surprising Plasticization Benefits in Natural Gas Upgrading using Polyimide Membranes, J. Membr. Sci., 593 (2020) 117430.
[17] B. Kraftschik, W. J. Koros, Cross-Linkable Polyimide Membranes for Improved Plasticization Resistance and Permselectivity in Sour Gas Separations, Macromolecules, 46 (2013) 6908-6921.
[18] S. Yi, B. Ghanem, Y. Liu, I. Pinnau, W. J. Koros, Ultraselective Glassy Polymer Membranes with Unprecedented Performance for Energy-Efficient Sour Gas Separation, Sci. Adv., 5 (2019) eaaw5459.
[19] B. Seoane, J. Coronas, I. Gascon, M. E. Benavides, O. Karvan, J. Caro, F. Kapteijn, J. Gascon, Metal-Organic Framework based Mixed Matrix Membranes: A Solution for Highly Efficient CO_2 Capture? Chem. Soc. Rev., 44 (2015) 2421-2454.
[20] J. Y. S. Lin, Molecular sieves for gas separation, Science, 353 (2016) 121-122.
[21] H. Furukawa, U. Muller, O. M. Yaghi, "Heterogeneity within Order" in Metal-Organic Frameworks, Angew. Chem. Int. Ed., 54 (2015) 3417-3430.
[22] B. Li, H. M. Wen, Y. Cui, W. Zhou, G. Qian, B. Chen, Emerging Multifunctional Metal-Organic Framework Materials, Adv. Mater., 28 (2016), 8819-8860.
[23] Y. Bai, Y. Dou, L. H. Xie, W. Rutledge, J. R. Li, H. C. Zhou, Zr-based Metal-Organic Frameworks: Design, Synthesis, Structure, and Applications, Chem. Soc. Rev., 45 (2016) 2327-2367.
[24] Lai, Z. P. Development of ZIF-8 Membranes: Opportunities and Challenges for Commercial Applications, Curr. Opin. Chem. Eng., 20 (2018) 78-85.
[25] C. Zhang, K. Zhang, L. Xu, Y. Labreche, B. Kraftschik, W. J. Koros, Highly Scalable ZIF-based Mixed-Matrix Hollow Fiber Membranes for Advanced Hydrocarbon Separations, AIChE J., 60 (2014) 2625-2635.
[26] J. E. Bachman, Z. P. Smith, T. Li, T. Xu, J. R. Long, Enhanced Ethylene Separation and Plasticization Resistance in Polymer Membranes Incorporating Metal-Organic Framework Nanocrystals, Nat. Mater., 15 (2016) 845.
[27] H. Furukawa, F. Gandara, Y. B. Zhang, J. Jiang, W. L. Queen, M. R. Hudson, O. M. Yaghi, Water Adsorption in Porous Metal–Organic Frameworks and Related Materials, J. Am. Chem. Soc., 136 (2014) 4369-4381.
[28] O. Yassine, O. Shekhah, A. H. Assen, Y. Belmabkhout, K. N. Salama, M. Eddaoudi, H_2S Sensors: Fumarate□Based fcu□MOF Thin Film Grown on a Capacitive Interdigitated Electrode. Angew. Chem. In. Ed., 55 (2016) 15879-15883.
[29] S. K. Mostakim, S. Bhowal, S. Biswas, Synthesis, Characterization, Stability, and Gas Adsorption Characteristics of a Highly Stable Zirconium Mesaconate Framework Material, Eur. J. Inorg. Chem., 20 (2015) 3317-3322.
[30] G. Liu, V. Chernikova, Y. Liu, K. Zhang, Y. Belmabkhout, O. Shekhah, C. Zhang, S. Yi, M. Eddaoudi, W. J. Koros, Mixed matrix formulations with MOF molecular sieving for key energy-intensive separations, Nat. Mater., 17 (2018) 283-289.
[31] Accelrys, I. Materials Studio. Accelrys Software Inc (2010).

[32] D. X. Xue, Y. Belmabkhout, O. Shekhah, H. Jiang, K. Adil, A. J. Cairns, M. Eddaoudi, Tunable Rare Earth Fcu-MOF Platform: Access to Adsorption Kinetics Driven Gas/Vapor Separations via Pore Size Contraction, J. Am. Chem. Soc., 137 (2015) 5034-5040.
[33] L. Guo, M. Wang, D. Cao, A Novel Zr□MOF as Fluorescence Turn□On Probe for Real□Time Detecting H_2S Gas and Fingerprint Identification, Small, 14 (2018) 1703822.
[34] P. M. Bhatt, Y. Belmabkhout, A. H. Assen, L.J. Weseliński, H. Jiang, A. Cadiau, D. X. Xue, M. Eddaoudi, Isoreticular Rare Earth Fcu-MOFs for the Selective Removal of H_2S from CO_2 Containing Gases, Chem. Eng. J., 324 (2017) 392-396.
[35] K. Adil, Y. Belmabkhout, R. S. Pillai, A. Cadiau, P. M. Bhatt, A. H. Assen, G. Maurin, M. Eddaoudi, Gas/Vapour Separation using Ultra-Microporous Metal–Organic Frameworks: Insights into the Structure/Separation Relationship, Chem. Soc. Rev., 46 (2017) 3402-3430.
[36] G. Wißmann, A. Schaate, S. Lilienthal, I. Bremer, A. M. Schneider, P. Behrens, Modulated Synthesis of Zr-fumarate MOF, Micropor. Mesopor. Mat., 152 (2012) 64-70.
[37] Y. Liu, Z. Chen, G. Liu, Y. Belmabkhout, K. Adil, M. Eddaoudi, W. J. Koros, Conformation-Controlled Molecular Sieving Effects for Membrane-Based Propylene/Propane Separation, Adv. Mater., 31 (2019) 1807513.
[38] M. L. Connolly, Solvent-Accessible Surfaces of Proteins and Nucleic Acids, Science, 221 (1983) 709-713.
[39] R. Semino, J. C. Moreton, N. A. Ramsahye, S. M. Cohen, G. Maurin, Understanding the origins of metal-organic framework/polymer compatibility, Chem. Sci., 9 (2018) 315.
[40] M. Z. Ahmad, M. Navarro, M. Lhotka, B. Zornaza, C. Tellez, W. M. de Vos, N. E. Benes, N. M. Konnertz, T. Visser, R. Semino, G. Maurin, V. Fila, J. Coronas, Enhanced Gas Separation Performance of 6FDA-DAM Based Mixed Matrix Membranes by Incorporating MOF UiO-66 and its derivatives, J. Membr. Sci., 558 (2018) 64-77.
[41] L. M. Robeson, The Upper Bound Revisited, J. Membr. Sci., 320 (2008) 390-400.
[42] L. Xu, C. Zhang, M. Rungta, W. Qiu, J. Liu, W. J. Koros, Formation of Defect-free 6FDA-DAM Asymmetric Hollow Fiber Membranes for Gas Separations, J. Membr. Sci., 459 (2014) 223-232.

Highlights

- Controlling molecular competitions among H_2S, CO_2, and CH_4 using MOFs
- Controlling plasticization benefits using MOFs
- The MOF/polymer hybrid membrane platform shows excellent natural gas sweetening performance under various realistic conditions

Declaration of interests

☒ The authors declare that they have no known competing financial interests or personal relationships that could have appeared to influence the work reported in this paper.

☐The authors declare the following financial interests/personal relationships which may be considered as potential competing interests: